

Coseismic slip distribution inversion with unequal weighted Laplacian smoothness constraints

Leyang Wang^{1,2,3} Xiong Zhao,^{1,2} Wenbin Xu,⁴ Lei Xie⁴ and Nan Fang⁵

¹Faculty of Geomatics, East China University of Technology, Nanchang 330013, China. E-mail: wleyang@163.com

²Key Laboratory of Watershed Ecology and Geographical Environment Monitoring, NASG, Nanchang 330013, China

³Key Laboratory for Digital Land and Resources of Jiangxi Province, Nanchang 330013, China

⁴Department of Land Surveying and Geo-Informatics, The Hong Kong Polytechnic University, Hong Kong, China

⁵School of Geosciences and Info-Physics, Central South University, Changsha 410083, China

Accepted 2019 March 7. Received 2019 February 24; in original form 2018 September 17

SUMMARY

In coseismic slip distribution inversion, the Laplacian smoothness constraint is used to avoid the rank deficiency of the coefficient Green matrix and ensure the smoothness among the patches of the fault plane. However, by introducing the classic Laplacian smoothness constraint, the inversion of the maximum slip is commonly underestimated. To better solve this problem, here we propose a new method of weighting to the Laplacian second-order smoothness matrices by the slip. The Laplacian smoothness constraint with unequal weights and the classic Laplacian constraint are used to carry out the simulation experiments. The simulation experiments show that the accuracy of the estimated maximum slip from our method is outperforming the classical Laplacian method by 12–19 per cent. Moreover, the estimations of the average slip and moment magnitude have been enhanced, which improved ranging from 4 to 12.5 per cent and 0.4 to 9 per cent over the inversion results of classic Laplacian smoothness constraint, respectively. In order to further validate the general applicability of the proposed method, we conduct the experiments in terms of the inversion of L'Aquila and Taiwan Meinong earthquakes. The maximum slip inversion results show that the inversion of Laplacian smoothness constraint with unequal weights are larger than that of the classic Laplacian smoothness constraint, which is consistent with the conclusion of simulation experiments. In addition, the parameters inversion results of the actual earthquake from the proposed method are in agreement with other studies which also indicate the feasibility and effectiveness of our method.

Key words: Inverse theory; Earthquake ground motions; seismic cycle; numerical modelling.

1 INTRODUCTION

In the research of epicentre mechanism, the source parameters of epicentre mainly include the strike, dip, length, width, the size and direction of slip of the fault. The source parameters of epicentre can be determined by seismic waves recorded from multiple seismic stations (e.g. Ji *et al.*, 2002, 2003; Ammon *et al.* 2005) and the deformation data of geodetic observations (e.g. Kasahara 1957; Savage & Hastie 1969). Although the source parameters of epicentre can be determined by processing and analysing the seismic wave data, it fails in reflecting the real energy released during the earthquakes with large seismic intensity (Ammon *et al.* 2005).

In recent years, the development of geodetic technology can compensate for the insufficiency of seismic wave observations. Moreover, geodetic technology can obtain the changes of the position of the Earth's surface before and after the earthquake more accurately. Geodetic data (e.g. InSAR and GPS data) are widely used in the field of seismic research (e.g. earthquake stress triggering, source

parameters of epicentre inversion, coseismic slip distribution inversion) due to its wide coverage, simple observation conditions and high precision (e.g. Funning *et al.* 2005; Liu *et al.* 2009; Delouis *et al.* 2010; Kobayashi *et al.* 2011; Pollitz *et al.* 2011; Tajima *et al.* 2013; Chen *et al.* 2014; Jiang *et al.* 2014; Diao *et al.* 2016; Wan *et al.* 2017; Xu *et al.* 2018; Zhao *et al.* 2018b). The research of coseismic slip distribution inversion can obtain parameters of epicentre effectively (e.g. magnitude, slip, slip angle, etc.), which play a major role in the analysis of post-earthquake deformation mechanisms and future earthquake risk assessment.

In coseismic slip distribution inversion, the relationship between surface deformation displacement and slip distribution parameters is linear. The common method of inverting slip parameters is the least-squares method with the smoothness constraint. The Linear relationship of slip distribution parameters and surface deformation depends on construction of Green function matrix. The elements of the Green's function matrix are consisting of the surface deformation displacements caused by the unit strike-slips and dip-slips

of each slip patches on the fault plane. In order to avoid ill-posed problems in the inversion process and to limit the varying range of gradient, some regularization methods such as Tikhonov regularization and von Karman regularization emerged (e.g. Tikhonov 1963; Tikhonov & Rudnicki 1977). In this paper, we utilize the Tikhonov regularization on account of the efficiency of computation comparing with von Karman Regularization (Amey *et al.* 2018). In the process of calculating with the Tikhonov regularization method, the determination of regularization parameters and regularization matrix is the key point. For the research of regularization matrix in coseismic slip distribution inversion, the regularization matrix constructed by classic Laplacian second-order smoothness matrix (abbreviation: LSC) is widely used (e.g. Desbrun *et al.* 1999; Jónsson *et al.* 2002; Maerten *et al.* 2005). However, the inversion results of classic Laplacian smoothness constraint would underestimate the maximum slip (e.g. Jiang *et al.* 2013; Fan *et al.* 2017). Fan *et al.* (2017) proposed an adaptive Laplacian smoothness constraint (abbreviation: ASC) method to deal with the inadaptability locating at the edge of patch on the fault. However, their method was complicated. Due to the above-mentioned problems, a method of weighting to Laplacian second-order smoothness matrices (abbreviation: WLSC) by slip is proposed in this paper.

Various approaches have been proposed for determining the regularization parameters, such as the ridge method (Arthur and Robert 1970; Wang 2003), the generalized cross-verification method (abbreviation: GCV; e.g. Allen 1974; Golub *et al.* 1979; Stone 1974), the L-curve method (e.g. Hansen 1992; Hansen & O'Leary 1993), the Helmert variance component estimation method (e.g. Helmert 1872; Grafarend 1985; Xu *et al.*, 2009, 2010), the U-curve method (e.g. Krawczyk-Stańdo & Rudnicki 2007; Chamorroservent *et al.* 2011; Arnrich *et al.* 2014; Zhong *et al.* 2014; Wang *et al.* 2018b) and the adaptive Tikhonov regularization with multiple regularization parameters (Wang *et al.* 2016). Although the GCV method can obtain a theoretically rigorous solution for the regularization parameters, it somewhat provides a flat curve that is difficult to locate the optimal regularization parameter (Wang, 2003). Although the ridge method has a low computing complexity, the major deficiency is that the regularization parameter obtained by this method is subjective. For the variance component estimation method, it treats the regularization parameter as the weight of the virtual observation data. The inversion results of this method may give rise to the negative variance (Amiri-Simkooei, 2016; Wang *et al.* 2018b). The calculation process of the adaptive regularization method is more complex than those of other methods (Wang *et al.* 2016). At present, the L-curve method is the most common method to determine regularization parameter in coseismic slip distribution inversion. The disadvantages of L-curve method are in two-fold: (1) An overreliance on the data fitting, and the solution process may not be convergent (Xu 1998); (2) Unable to read the size of the regularization parameter directly from the L-curve according to the horizontal and vertical axis. In response to the above situation, the regularization parameters of this paper would be obtained by the U-curve method (Wang *et al.* 2018b).

The reminder of this paper is organized as follows: In Section 2, the basic principles of the LSC, WLSC and the U-curve method for determining regularization parameters are introduced. In Section 3, a systematic simulation experiments were designed, including the inversion experiments of the coseismic slip distribution with different fault depths and multislapping zones, and comparison experiments. In Section 4, the WLSC were applied to the inversion of coseismic slip distributions on 2009 April 6 in L'Aquila earthquake and on 2016 February 6 in Taiwan's Meinong earthquake.

In Section 5, we set a simple experiment to compare the method of the paper with Bayesian method (Bagnardi & Hooper, 2018) and summarize the full text.

2 BASIC PRINCIPLE OF LAPLACIAN SMOOTHNESS CONSTRAINT WITH UNEQUAL WEIGHTS

2.1 Classic Laplacian smoothness constraint

In the coseismic slip distribution inversion, the relationship between the coseismic displacements of surface and the slip parameters of fault plane is linear, which can be expressed as

$$\mathbf{d} = \mathbf{Gm} + \boldsymbol{\varepsilon}, \quad (1)$$

where \mathbf{d} represents surface deformation data, $\boldsymbol{\varepsilon}$ is the observation error of surface deformation data, \mathbf{m} is coseismic sliding parameter and \mathbf{G} is the corresponding Green's matrix (Yagi & Fukahata 2011), which can be expressed as

$$\mathbf{G} = \begin{bmatrix} ss_1^1 & ds_1^1 & ss_1^2 & ds_1^2 & \dots & ss_1^n & ds_1^n \\ ss_2^1 & ds_2^1 & ss_2^2 & ds_2^2 & \dots & ss_2^n & ds_2^n \\ \dots & \dots & \dots & \dots & \dots & \dots & \dots \\ ss_k^1 & ds_k^1 & ss_k^2 & ds_k^2 & \dots & ss_k^n & ds_k^n \end{bmatrix}. \quad (2)$$

The fault plane is usually subdivided into n rectangular patches in coseismic slip distribution inversion. According to the theory of dislocations (Okada, 1985, 1992; Sun *et al.* 1996), the deformation of the k observation points on the surface caused by the unit strike-slip and the dip-slip of each fault patch is calculated. Moreover, the Green function matrix \mathbf{G} of $k \times 2n$ is constructed as shown in formula (2). If the slip distribution solution is directly calculated by the least-squares method, the instability of the slip distribution solution will occur because the Green matrix is seriously ill-posed. To solve the above problem, LSCs are often used to impose on dislocations among each patches of fault plane. The Laplace operator of fault plane is shown in Fig. 1. Taking the fault patch S_0 as an example, the second-order Laplace operator can be expressed as follows:

$$\nabla^2 S = \frac{S_1 - 2S_0 + S_3}{d_1^2} + \frac{S_2 - 2S_0 + S_4}{d_2^2}, \quad (3)$$

where $S_i (i = 1, 2, 3, 4)$ represents the slip size of the patches around the fault patch S_0 . d_1, d_2 are the distance between adjacent fault patches along the directions of tendency and strike, respectively. $\nabla^2 S$ is defined as a smoothness index. We construct the constraint equations by assigning $\nabla^2 S = \mathbf{0}$ to all patches on the fault plane. Therefore, a new coseismic slip distribution inversion equation is obtained by combining with formula (1).

$$\begin{bmatrix} \mathbf{d} \\ \mathbf{0} \end{bmatrix} = \begin{bmatrix} \mathbf{G} \\ \alpha \mathbf{H} \end{bmatrix} \mathbf{m}, \quad (4)$$

where the $\mathbf{0}$ matrix denotes a virtual observation matrix, \mathbf{H} and α represent the Laplacian smoothness matrix and regularization parameter, respectively.

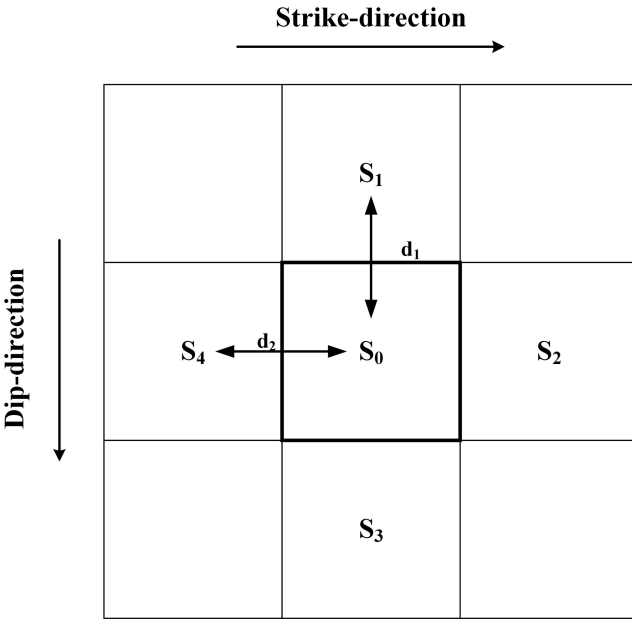


Figure 1. Partial Laplacian operator schematic of fault rupture.

2.2 Laplacian smoothness constraint with unequal weights

For convenience, we assume that $d_1 = d_2 = d$, the formula (3) can be expressed as follows (Fan *et al.* 2017)

$$\frac{S_1 + S_2 + S_3 + S_4 - 4S_0}{d^2} = 0. \quad (5)$$

After further simplification, the formula (5) can be rewritten as

$$S_0 = \frac{S_1 + S_2 + S_3 + S_4}{4}. \quad (6)$$

As discussed before, the classic Laplacian constraint underestimates the maximum slip, thus, this paper proposes a method by weighting to classic Laplacian second-order smoothness matrix. The main idea is to invert the large slip distances of middle fault patches via increasing the weights of slip among the surrounding patches. If we assume that S_0 is the maximum slip patch (see Fig. 1), the maximum slip can be tuned proportionally by reweighting the surrounding patches $S_i (i = 1, 2, 3, 4)$.

Based on the above theory, the paper proposes a new weighting method by using the values of slip, and the specific weighting process is as follows:

(1) The initial slip distribution solution is obtained by using the LSC for slip distribution inversion.

$$\mathbf{m} = (\mathbf{G}^T \mathbf{G} + \alpha^2 \mathbf{R})^{-1} \mathbf{G}^T \mathbf{d}, \quad (7)$$

where $\mathbf{R} = \mathbf{H}^T \mathbf{H}$ is the regularization matrix. The elements of \mathbf{m} are composed of the strike-slip and dip-slip of each patches on the fault

plane, which can be expressed as $\mathbf{m} = \begin{bmatrix} m_{11} \\ m_{12} \\ \vdots \\ m_{n1} \\ m_{n2} \end{bmatrix}$. n indicates the total number of slip patches on the fault plane. $m_{11}, m_{21} \dots m_{n1}$ are the amount of strike-slip of each patch, $m_{12}, m_{22} \dots m_{n2}$ are the amount of dip-slip of each patch.

(2) Calculate the amount of slip of each patch on the fault plane.

$$m_{iz} = (m_{i1}^2 + m_{i2}^2)^{1/2} (i = 1, 2 \dots n) \quad (8)$$

m_{iz} is the sum-slip of the i th fault patches, let $\mathbf{m}_z = \begin{bmatrix} m_{1z} \\ \vdots \\ m_{nz} \end{bmatrix}$

represents the column vector constructed by the sum-slip elements of each fault patches.

(3) Calculate the maximum sum-slip of the fault patches on the fault plane m_{\max} .

$$m_{\max} = \max(\mathbf{m}_z) \quad (9)$$

(4) Take m_{\max} as the unit weight and weigh each slip patch of the fault plane.

$$p_i = \frac{m_{\max}}{m_{iz}}, \quad (10)$$

where p_i represents the weights of the i th patch on the fault plane.

(5) Weight to classic Laplacian second-order smoothness matrix.

The elements of the classic Laplacian second-order smoothness matrix are consisting of the surface deformation displacements caused by the unit strike-slips and dip-slips of each fault patch on the fault plane. In this paper, it is assumed that elements of the same slip patch in Laplacian second-order smoothness matrix have identical weights. The weight value is also equal to the corresponding weight of the slip patch. The weight matrix of Laplacian second-order smoothness matrix can be expressed as follows:

$$\mathbf{P} = \begin{bmatrix} p_1 & 0 & 0 & 0 & 0 & 0 \\ 0 & p_1 & 0 & 0 & 0 & 0 \\ 0 & 0 & \ddots & 0 & 0 & 0 \\ 0 & 0 & 0 & \ddots & 0 & 0 \\ 0 & 0 & 0 & 0 & p_n & 0 \\ 0 & 0 & 0 & 0 & 0 & p_n \end{bmatrix}. \quad (11)$$

Through the above method, we can determine the weights of the fault patches which are in inverse proportion to the slip. Consequently, the neighbours' weights surrounding the maximum slip path are larger than it. Thus, the problem of underestimating the maximum slip by the classic Laplacian constraint could be improved according to the formula (6).

After the Laplacian second-order smooth matrix has weighted, the solution of coseismic slip distribution with WLSC can be expressed as follows:

$$\mathbf{m} = (\mathbf{G}^T \mathbf{G} + \alpha^2 \mathbf{P}^T \mathbf{P} \mathbf{H})^{-1} \mathbf{G}^T \mathbf{d}, \quad (12)$$

where \mathbf{P} denotes a matrix of weights corresponding to elements in the Laplacian second-order smoothness matrix. Since the size of the inversion model roughness has changed, the corresponding regularization parameter α needs to be recalculated. In this paper, regularization parameters α are calculated by the U-curve method.

2.3 U-curve method

U-curve method is similar to L-curve method in determining the regularization parameter. By plotting the $U(\alpha) - \alpha$ curve according to the formula (13), the U-curve method obtains a set of $U(\alpha)$ values based on different α values. Make $U(\alpha)$ as the ordinate and α as the abscissa, and fitting of them can get a $U(\alpha) - \alpha$ curve. We can determine the regularization parameter by finding a local

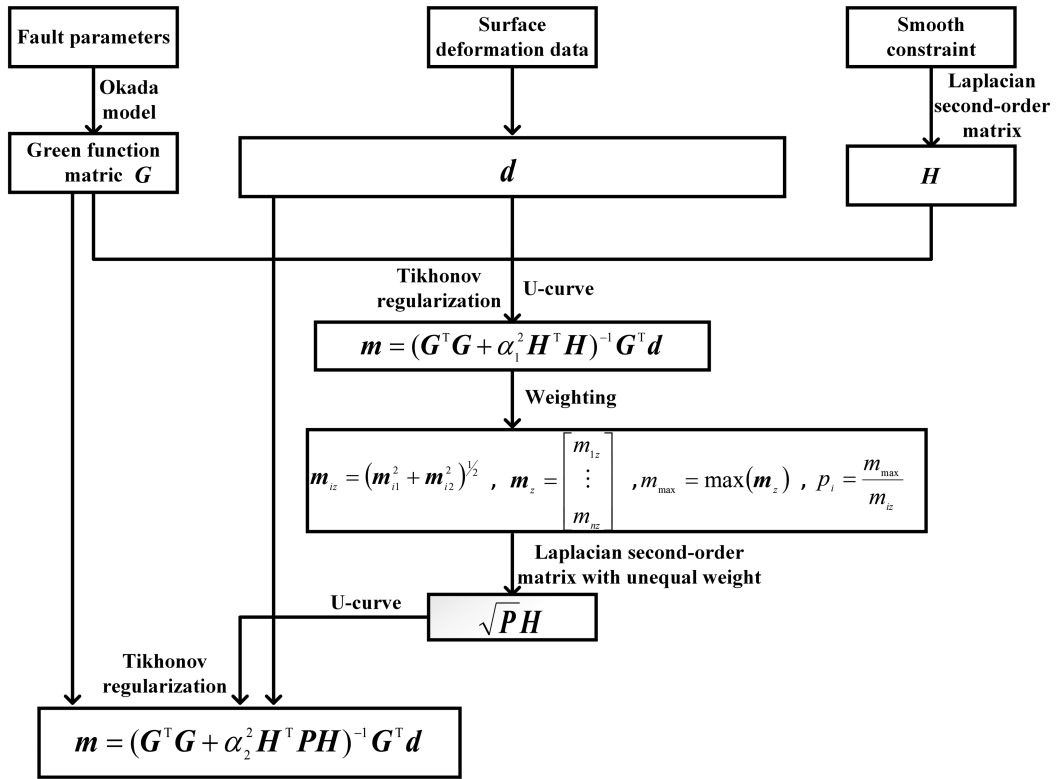


Figure 2. The flow chart of coseismic slip distribution inversion of Laplacian smoothing constraint with unequal weights.

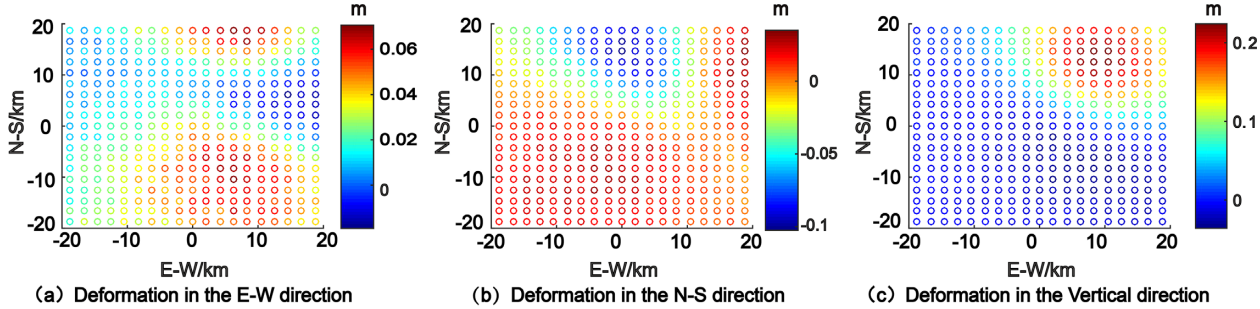


Figure 3. The simulated observation data of GPS in simulation experiment 1.

Table 1. The three schemes of simulated experiment 1.

Schemes	Methods
Scheme 1	The U-curve method is used to determine the regularization parameters and the slip distribution inversion is performed with classic Laplacian smoothing constraints.
Scheme 2	The U-curve method is used twice to determine the regularization parameters, and the slip distribution inversion is performed by using Laplacian smooth constraints with unequal weights.
Scheme 3	The U-curve method is used once to determine the regularization parameters, and the slip distribution inversion is performed using Laplacian smooth constraints with unequal weights.

maximum in it. To be specific, the local maximum is close to the left vertical part of the U-curve (e.g. Krawczyk-Stańdo & Rudnicki 2007; Chamorroservent et al. 2011; Arnrich et al. 2014; Zhong et al. 2014; Wang et al. 2018b). The U-curve function can be defined as follows.

$$U(\alpha) = \frac{1}{\|Gm - d\|^2} + \frac{1}{\|Hm\|^2}. \quad (13)$$

In formula (13), $\|Gm - d\|^2 = \sum_{i=1}^r \frac{\alpha^4 \beta_i^4 \theta_i^2}{(\sigma_i^2 + \alpha^2 \beta_i^2)^2}$ and $\|Hm\|^2 =$

$\sum_{i=1}^r \frac{\sigma_i^2 \beta_i^2 \theta_i^2}{(\sigma_i^2 + \alpha^2 \beta_i^2)^2}$ (e.g. Wang et al. 2018b), where $\theta = v^T d$. v is the left-hand side singular value matrix after the singular value decomposition of the Green matrix G . $\sigma_1 \geq \sigma_2 \dots \geq \sigma_r > 0$ are the singular values of the Green matrix G and $\beta_1 \geq \beta_2 \dots \geq \beta_r > 0$ are the singular values of the Laplacian matrix. It can be seen from the definition of U-curve method that the regularization parameter determined by the U-curve method does not need curve fitting and extra calculations. Therefore, the U-curve method is better than the L-curve method in some aspects (Wang et al. 2018b).

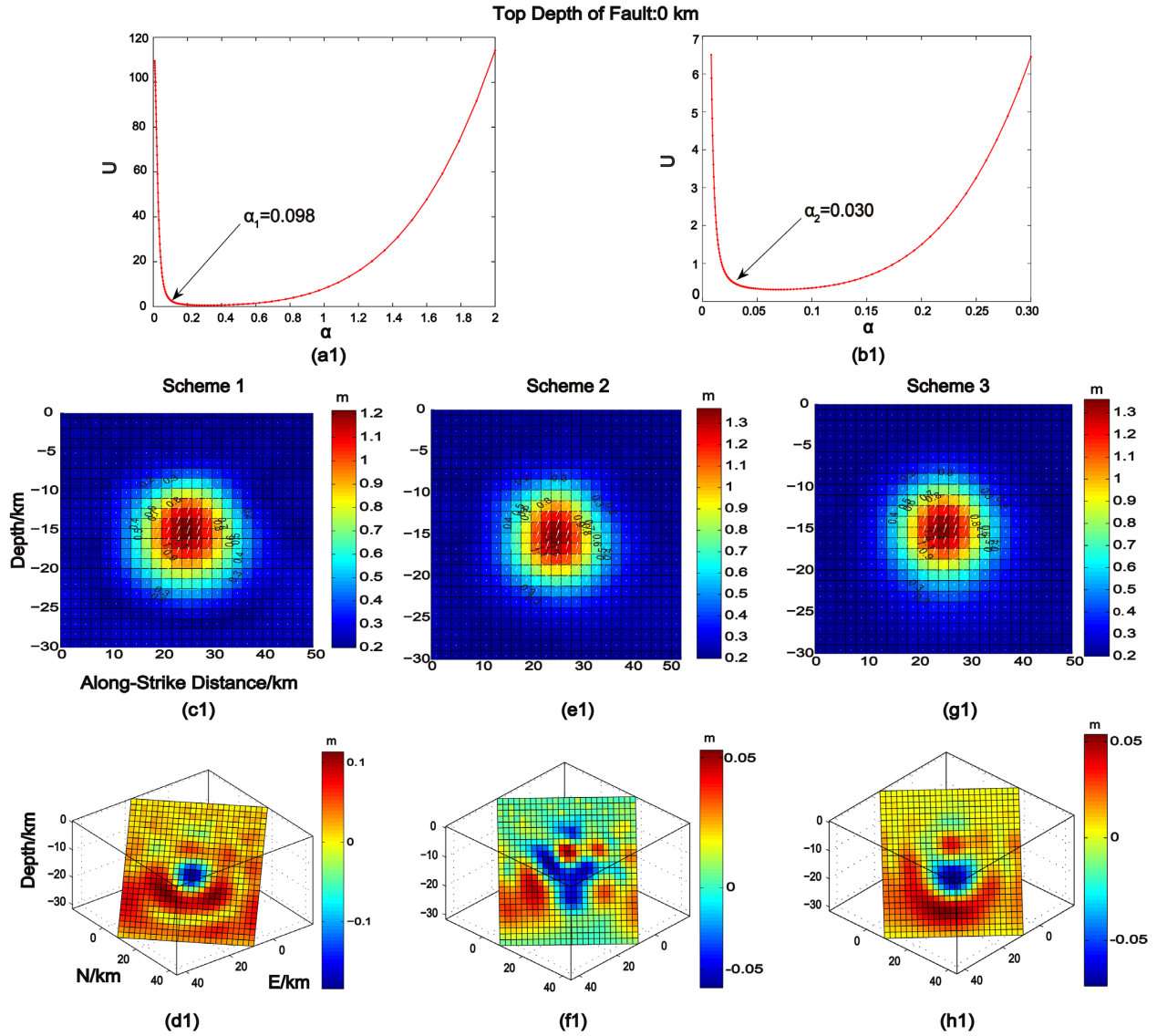


Figure 4. The slip distribution inversion results with the 0 km fault top depth in different schemes. (a1–b1) The regularization parameters determined by the U-curve method of the fault depth is 0 km. (c1–d1) The slip distribution inversion results and residual distribution of the 0 km's fault top depth by scheme 1. (e1–f1) The slip distribution inversion results and residual distribution of the 0 km's fault top depth by scheme 2. (g1–h1) The slip distribution inversion results and residual distribution of the 0 km's fault top depth by scheme 3.

In summary, the inversion process of coseismic slip distribution of WLSC is shown in Fig. 2.

In the seismic slip distribution inversion of earthquakes, the root mean square errors (abbreviation: RMS) between the observed values and the inverse values of dislocation model are often used as one of the metrics for the evaluation. It can be expressed as follows:

$$RMS = \sqrt{\frac{\sum_{i=1}^n P_i (\mathbf{d}_i - \mathbf{c}_i)^2}{n}}. \quad (14)$$

n represents the number of observations; \mathbf{d} and \mathbf{c} represent the magnitude of the surface observations and model inversion values; P represents the weighting matrix of the observations.

In order to evaluate that the performance of the proposed WLSC method, we conduct experiments both on the system's simulation data and actual seismic data (e.g. the 2009 April 6 L'Aquila M_w 6.3 and the 2016 February 6 Meinong and Taiwan M_w 6.4).

3 SIMULATION EARTHQUAKE EXPERIMENTS

In order to evaluate the performance of our method, we simulated experiments in the following three aspects: (1) Simulating coseismic slip distribution inversion with different fault top depths: 0 km, -2 km, -15 km. (2) Simulating coseismic slip distribution inversion experiment in a dual-slipping area. (3) Comparing experiment with ASC inversion method (Fan *et al.* 2017). The advantages and insufficiency of the WLSC and the ASC inversion of the coseismic slip distribution were compared.

3.1 Simulated seismic experiment 1

In simulation experiment 1, the simulated fault plane geometry parameters are set as follows: the geometry centre of fault plane is $X = 0$ km, $Y = 0$ km. The top depths of fault are 0 km, -2 km, -15 km. The length and width of fault plane are both 50 km. The angle of

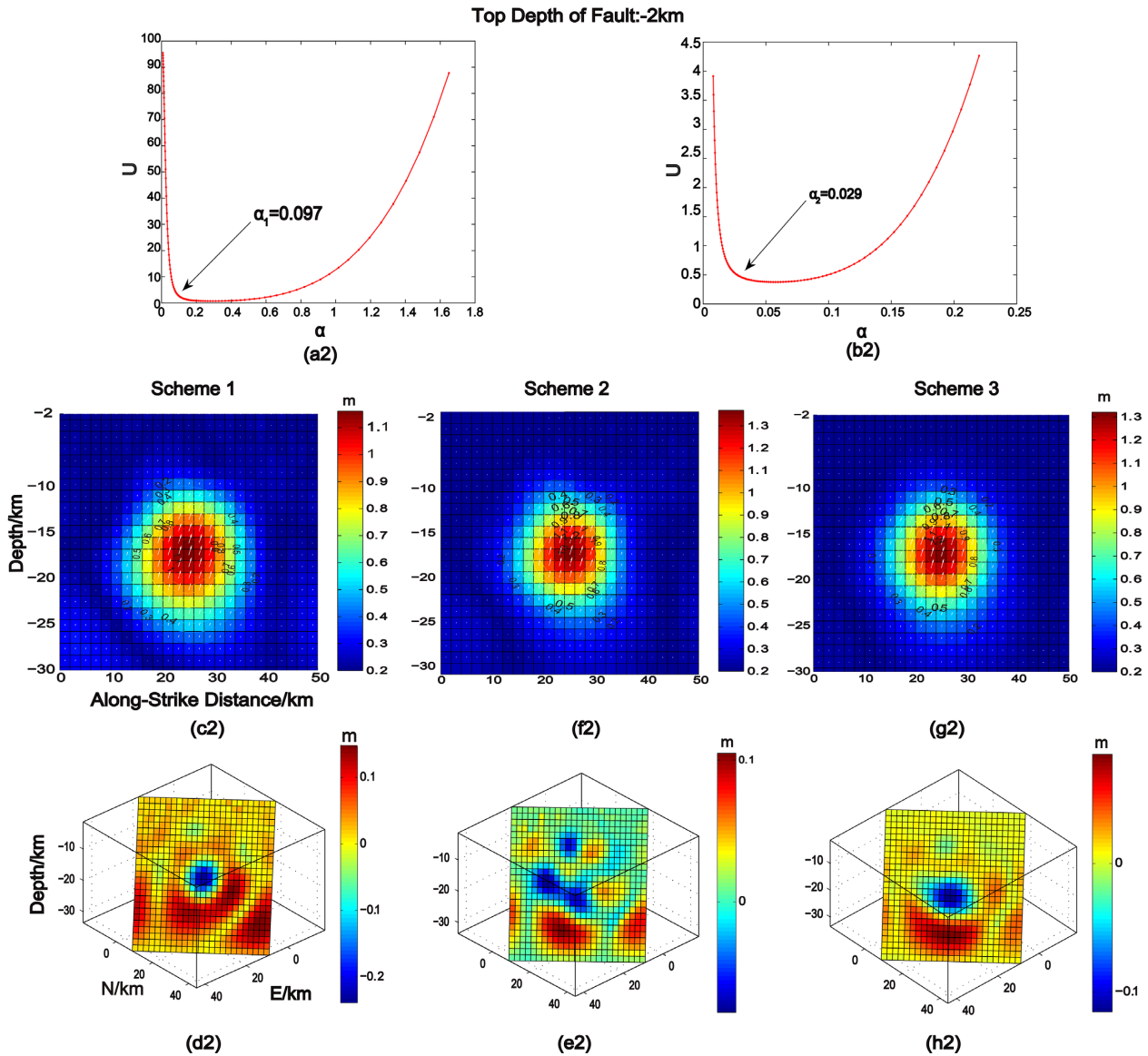


Figure 5. The slip distribution inversion results with the -2 km fault top depth in different schemes. (a2–b2) The regularization parameters determined by the U-curve method of the fault depth is -2 km . (c2–d2) The slip distribution inversion results and residual distribution of the -2 km 's fault top depth by scheme 1. (e2–f2) The slip distribution inversion results and residual distribution of the -2 km 's fault top depth by scheme 2. (g2–h2) The slip distribution inversion results and residual distribution of the -2 km 's fault top depth by scheme 3.

strike and dip of the fault plane are 135° and 40° , respectively. The slip angle of the fault plane is 60° . The simulated GPS three directions observation data are shown in Fig. 3. The 625 observation points are simulated, and each point is evenly distributed within 25 km of the epicentre. Simultaneously, the $N(0, 3^2\text{mm}^2)$ observation error are imposed to the GPS points (Yagi Y & Fukahata Y, 2008). In simulation experiment 1, three schemes of Table 1 were used to perform the slip distribution inversion.

As discussed in Section 2, the proposed WLSC method will determine the regularization parameters twice by the U-curve method. In order to validate the independence between the inversion results and the size of regularization parameters, we add a comparison as scheme 3 in which the U-curve method is merely utilized once. The inversion of coseismic slip distributions was performed by using the three schemes, in which the slip distribution inversion results by three schemes in different fault top depths (0 km , -2 km , -15 km)

and the regularization parameters which were determined by U-curve method are shown in Figs 4–6.

The detailed parameters of the slip distribution inversion by three schemes in different fault top depths (0 km , -2 km and -15 km) of simulation experiment 1 are listed in Table 2.

In simulation experiment 1, scheme 3 is to investigate the relationship between the maximum slip inversion result of WLSC and the varying matrix size of regularization parameters. It can be seen from Table 2 that the regularization parameters of scheme 3 is consistent with scheme 1, and the maximum slip inversion result of scheme 3 is significantly improved. Therefore, it can prove that the redetermination of regularization parameters (i.e. estimating twice by the U-curve method) does not impose the inversion result. Since the scheme 3 of this paper is unreasonable in theory, we only considered the schemes 1 and 2 in the later data analysis and experiments 2 and 3.

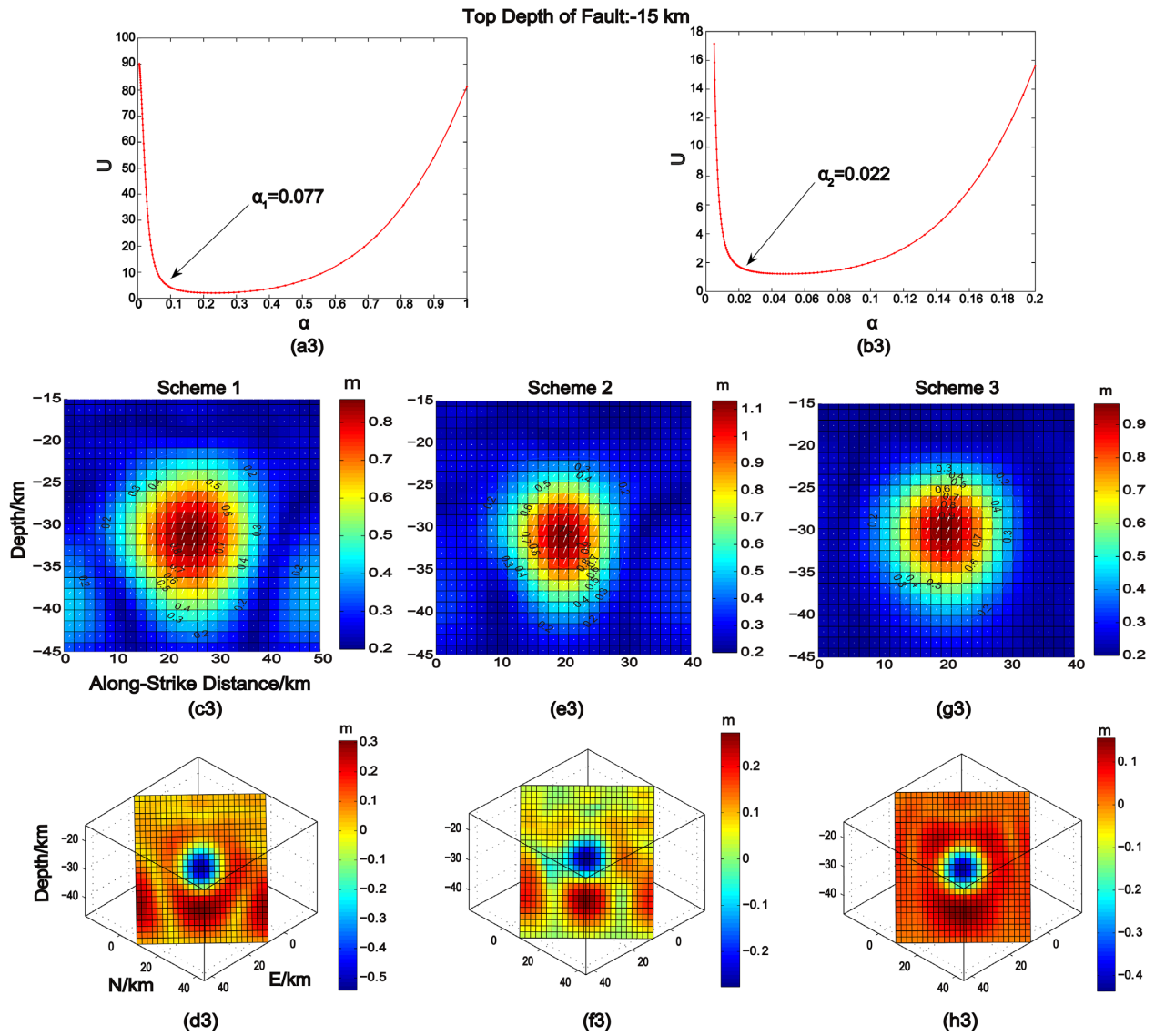


Figure 6. The slip distribution inversion results with the -15 km fault top depth in different schemes. (a3–b3) The regularization parameters determined by the U-curve method of the fault depth is -15 km . (c3–d3) The slip distribution inversion results and residual distribution of the -15 km 's fault top depth by scheme 1. (e3–f3) The slip distribution inversion results and residual distribution of the -15 km 's fault top depth by scheme 2. (g3 – h3) The slip distribution inversion results and residual distribution of the -15 km 's fault top depth by scheme 3.

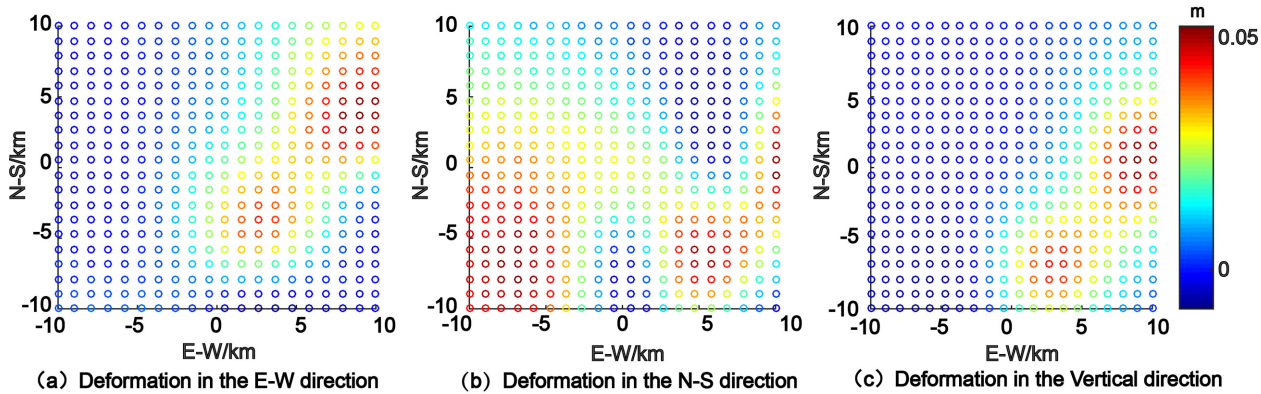
Table 2. The coseismic slip distribution inversion results of simulated experiment 1.

Values	Top depth/km	Schemes	Regularization parameters	Max slip/m	Mean slip/m	Slip angle at max slip (°)	Moment magnitude/ (M_w)	Seismic moment /($10^{19}\text{ N}\cdot\text{m}$)	RMS /(m)
Analogue values	//	//	//	1.400	0.1477	60	6.6631	1.1081	//
Inversion values	0	Scheme 1	0.098	1.2311	0.1765	60.4410	6.7146	1.3240	0.0029
	0	Scheme 2	0.098/0.030	1.3984	0.1608	59.8460	6.6876	1.2060	0.0029
	0	Scheme 3	0.098/0.098	1.3672	0.1565	60.7080	6.6797	1.1736	0.0029
	-2	Scheme 1	0.097	1.1613	0.1781	61.7469	6.7172	1.3359	0.0029
	-2	Scheme 2	0.097/0.029	1.3696	0.1648	62.0174	6.6946	1.2357	0.0029
	-2	Scheme 3	0.097/0.097	1.3197	0.1576	62.3773	6.6818	1.1822	0.0029
	-15	Scheme 1	0.077	0.8613	0.2177	60.7347	6.7752	1.6325	0.0030
	-15	Scheme 2	0.077/0.022	1.1318	0.2108	60.1477	6.7659	1.5807	0.0030
	-15	Scheme 3	0.077/0.077	0.9630	0.1738	60.1762	6.7100	1.3034	0.0030

Table 3. Comparison of the parameters of inversion results by schemes 1 and 2 with the analogue value of simulated experiment 1.

Top depth/km	schemes	Max slip/m	Mean slip/m	Moment magnitude/(Mw)
0	Scheme 1	0.1689	0.0288	0.0515
0	Scheme 2	0.0016	0.0131	0.0245
0	Improved*	11.95 per cent	10.63 per cent	0.41 per cent
-2	Scheme 1	0.2387	0.0304	0.0541
-2	Scheme 2	0.0304	0.0171	0.0315
-2	Improved*	14.88 per cent	9.00 per cent	0.34 per cent
-15	Scheme 1	0.5387	0.07	0.1121
-15	Scheme 2	0.2682	0.0631	0.0469
-15	Improved*	19.32 per cent	4.67 per cent	9.79 per cent

Note: Improved* = $\left| \frac{D_1 - D_2}{D} \right|$, D_1 represents the D-values between the parameter values of inversion and the analogue values of scheme 1, D_2 represents the D-values between the parameter values of inversion and the analogue values of scheme 2, D represents the analogue value.

**Figure 7.** The simulated observation data of GPS three-direction in simulation experiment 2.**Table 4.** The coseismic slip distribution inversion results of simulated experiment 2.

Schemes	Regularization parameters/(\alpha)	Max slip/m	Mean slip/m	Moment magnitude /(Mw)	Seismic moment/(10 ¹⁷ N·m)	RMS/(mm)
Analogue values	//	1	0.06	5.8716	7.2	//
Scheme 1	0.069	0.3676	0.0830	5.9657	9.9658	0.511
Scheme 2	0.069/0.021	0.5037	0.0755	5.9381	9.0609	0.376

Table 5. Comparison of the parameters of inversion results by schemes 1 and 2 with the analogue value of simulated experiment 2.

Schemes	Max slip/m	Mean slip/m	Moment magnitude /(Mw)
Scheme1	0.6324	0.023	0.0941
Scheme2	0.4963	0.0075	0.0665
Improved*	13.61 per cent	12.5 per cent	2.74 per cent

Note: Improved* = $\left| \frac{D_1 - D_2}{D} \right|$, D_1 represents the D-values between the parameter values of inversion and the analogue values of scheme 1, D_2 represents the D-values between the parameter values of inversion and the analogue values of scheme 2, D represents the analogue value.

The D-values (i.e. the difference between the inversion values and the analogue values) between the parameters inversion results of slip distribution by schemes 1 and 2 with analogue values, and the improvement of the scheme 2 are shown in Table 3.

In Tables 2 and 3, it can be easily seen that with the gradual deepening of the fault depth, the accuracy of the coseismic slip distribution of the two schemes is gradually reduced. For the maximum

slip at 1.4 m, the D-values from the inversion results of LSC is about 0.15–0.3 m. It is worthy to be noted that the D-value reaches a maximum at 0.5 m with the increasing depth value. This suggests that the classic LSC method cannot obtain a reliable inversion result. However, the D-values from the proposed WLSC method is in the range of 0.002–0.03 m, with a maximum difference of 0.1 m. Moreover, the maximum slip inversion results of WLSC has improved

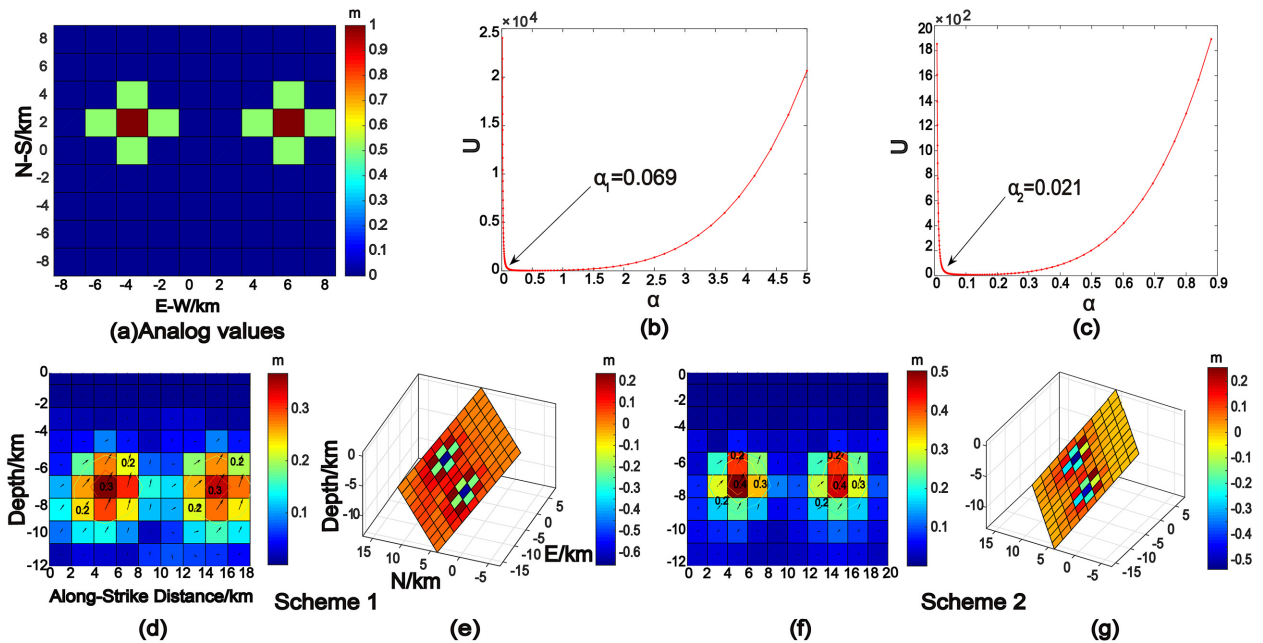


Figure 8. The slip distribution inversion results of simulation experiment 2. (a) The distribution of analogue slip value. (b,c) The regularization parameters are determined by the U-curve method of simulation experiment 2. (d,e) The slip distribution inversion results and recoverability distribution by the scheme 1. (f,g) The slip distribution inversion results and recoverability distribution by the scheme 2.

Table 6. The three schemes of simulated experiment 3.

Schemes	Methods
Scheme 4	The variance component estimation method is used to determine the regularization parameters, and the slip distribution inversion is performed with adaptive Laplacian smoothing constraints.
Scheme 5	The variance component estimation method is used twice to determine the regularization parameters, and the slip distribution inversion is performed with adaptive Laplacian smoothing constraints.
Scheme 2	The U-curve method is used twice to determine the regularization parameters, and the slip distribution inversion is performed by using Laplacian smooth constraints with unequal weights.

Table 7. The coseismic slip distribution inversion results of simulated experiment 3.

Schemes	Regularization parameters/(α)	Max slip/(m)	Mean slip/(m)	Moment magnitude /(M_w)	Seismic moment/(10^{17} N·m)	RMS/(mm)
Analogue values	//	10	3.7805	7.1885	6.68049	//
Scheme 4	//	≈ 9.6	//	//	//	//
Scheme 5	0.041/0.102	10.20	3.7810	7.1886	6.8058	2.6
Scheme 2	0.028/0.004	9.9789	3.7806	7.1886	6.8050	2.5

Table 8. Comparison of the parameters of inversion results by schemes 5 and 2 with the analogue value of simulated experiment 3.

Schemes	Max slip/(m)	Mean slip/(m)	RMS/(M_w)
Scheme 5	0.20	0.0005	2.6
Scheme 2	0.0211	0.0001	2.5
Improved*	17.89 per cent	0.01 per cent	4 per cent

Note: Improved* = $|\frac{D_5 - D_2}{D}|$, D_5 represents the D-values between the parameter values of inversion and the analogue values of scheme 5, D_2 represents the D-values between the parameter values of inversion and the analogue values of scheme 2, D represents the analogue value.

the range from 11 to 19 per cent than the inversion results of LSC. In addition, from the colour bar of the recoverability distribution maps of Figs 4–6 (d1), (d2) and (d3), (f1), (f2), (f3), it can be seen that the residual distribution of the inversion slip error of scheme 2 is smaller than that of scheme 1. Therefore, it is further shown

that the inversion results of the scheme 2 is more accurate. For the slip angle at the maximum slip, the inversion results are close to the analogue values, we will not further analyse the slip angle in this paper.

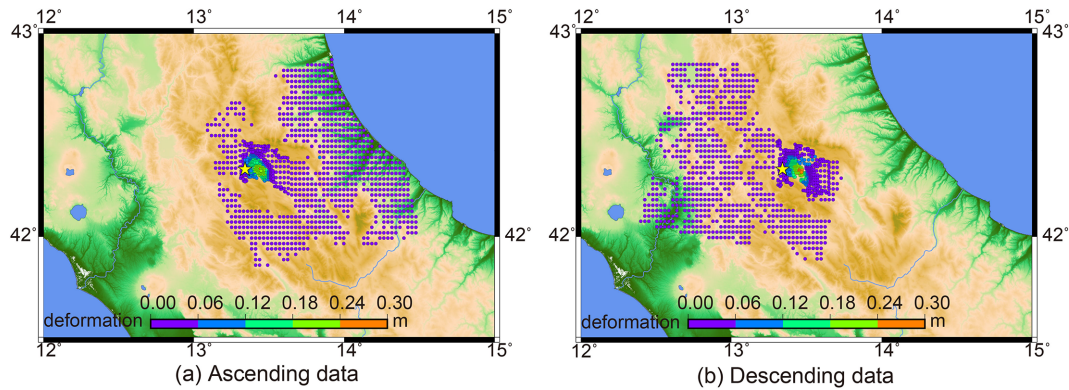


Figure 9. The InSAR data of L'Aquila earthquake. (a) The ascending data of L'Aquila earthquake. (b) The descending data of L'Aquila earthquake.

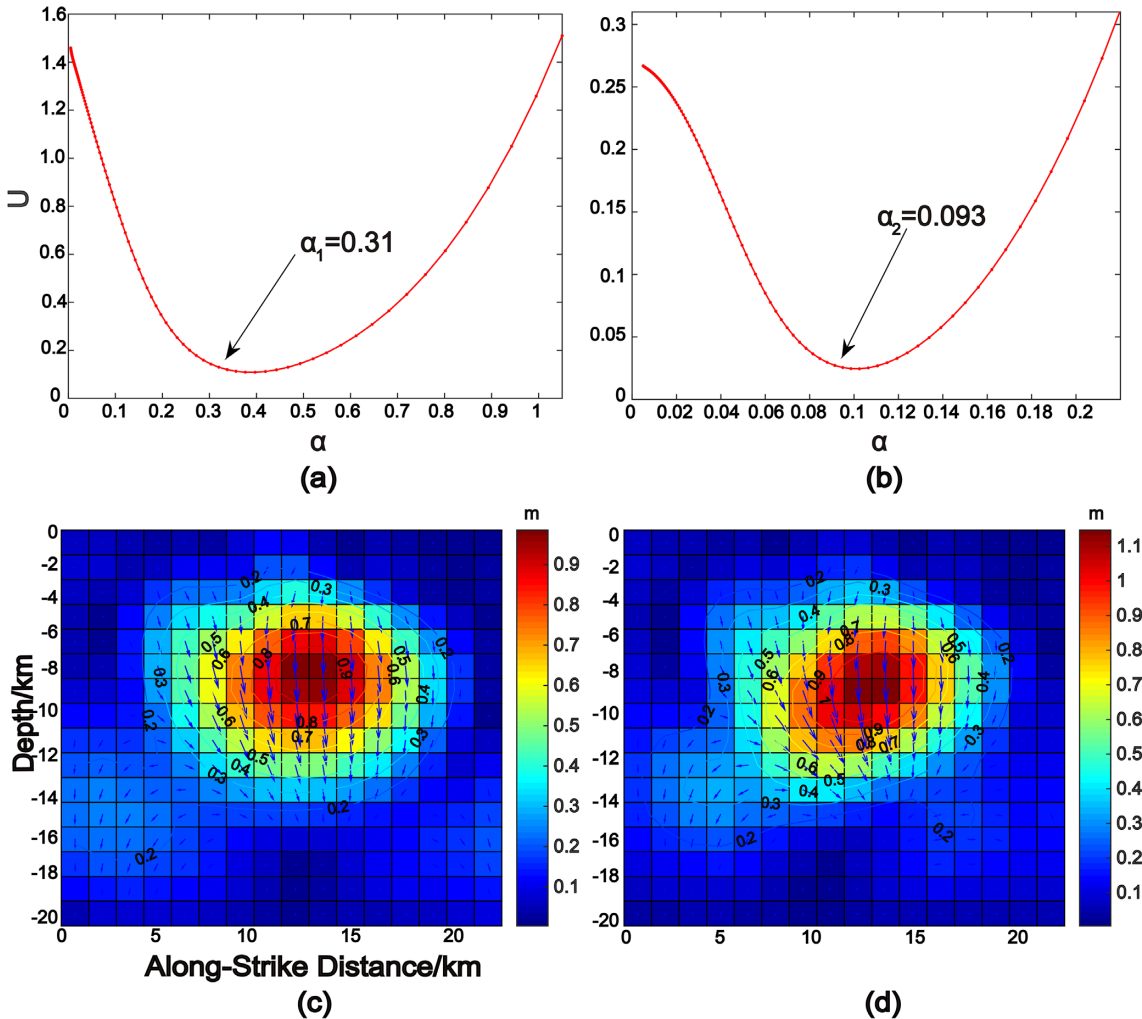


Figure 10. The slip distribution inversion results of L'Aquila earthquake. (a,b) The regularization parameters are determined by the U-curve method of L'Aquila earthquake. (c,d) The slip distribution inversion results of L'Aquila earthquake by schemes 1, 2.

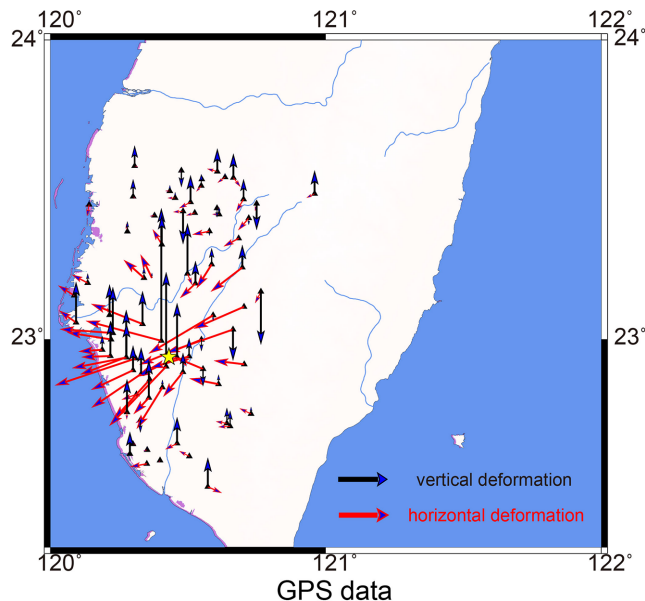
3.2 Simulated seismic experiment 2

In experiment 2, we simulate a fault with multimain sliding area for the coseismic slip inversion to further demonstrate the effectiveness of our method. Taking a double main sliding area as an instance, the geometry of fault is in the following: The geometry centre of fault plane is $X = 0\text{ km}$, $Y = 0\text{ km}$. The top depth of fault is 0 km . The length and width of fault plane are

both 20 km . The angle of strike and dip of the fault plane are 50° and 45° , respectively. The slip angle of fault plane is 45° . The simulated GPS three directions observation data are shown in Fig. 7. The 400 observation points are simulated, and all points are uniformly distributed within 10 km of the epicentre. Moreover, we add a Gaussian noise at $N(0, 3^2\text{mm}^2)$ to the simulated GPS observations.

Table 9. The various source parameters for L'Aquila earthquake.

Seismic parameters	Scheme 1	Scheme 2	Wang <i>et al.</i> (2017a)	Wen <i>et al.</i> (2012)	Walters <i>et al.</i> (2009)	Anzidei <i>et al.</i> (2009)	Cheloni <i>et al.</i> (2010)	USGS
Max slip/m	0.99	1.15	0.95	1.07	0.66	0.49	1.1	//
Mean slip angle/(°)	-93.2	-93.5	-96.4	-102.8	-105	-98	-98.5	//
Moment magnitude /(M_w)	6.34	6.36	6.34	6.32	6.23	6.32	6.36	6.29
Seismic moment//(10 ¹⁸ Nm)	3.62	3.9	3.63	3.43	2.8	3.2	3.9	3.4

**Figure 11.** The GPS observation data of Meinong earthquake.

The inversion of the coseismic slip distribution is carried out by using the schemes 1, 2 in the simulation experiment 1. The analogue value of slip is shown in Fig. 8(a). The regularization parameters were determined by the U-curve method are shown in Fig. 8(b,c). The results of slip distribution inversion of two schemes are shown in Figs 8(d)–(f).

The parameters inversion results of slip distribution of two schemes are shown in Table 4. The D-values between the parameters inversion results of two schemes with the analogue values, and the improvement of scheme 2 compared to the scheme 1 are shown in Table 5.

The statistics of the result in Tables 4 and 5 indicate that for the faults with complex multisliding area, the parameters inversion accuracy of WLSC still has more improvement than that of LSC. The maximum slip, average slip and moment magnitude has increased by 13.61, 12.5 and 2.74 per cent, respectively. Moreover, from the inversion results of root mean square error in Table 4, it can be concluded that the inversion result accuracy of WLSC is higher than LSC. In addition, from Figs 8 (a), (d), (e), (f), (g), it can be seen that the result of slip distribution inversion of scheme 2 is closer to the analogue value than the scheme 1 (Fig. 8a), it is further shown that the results of coseismic slip distribution inversion result of WLSC are more accurate.

3.3 Simulated seismic experiment 3

Fan *et al.* (2017) proposed an adaptive smoothness constraint method. Since the calculation process of ASC method is complicated, we conduct the comparing experiments by their data other than the experiments 1 and 2. Specifically, the fault parameters were set according to Fan *et al.* (2017) simulation experiment 1 as follows: the geometry centre of fault plane is X = 0 km, Y = 0 km. The top depth of fault is 0 km. The length and width of the fault plane are 20, 30 km. The angle of strike and dip of the fault plane are 90° and 45°, respectively. In simulation experiment 3, three schemes of Table 6 were used to perform the slip distribution inversion [Scheme 4 is from Fan *et al.* (2017) and the calculation results are from fig. 12 in Fan *et al.* (2017)].

The results of coseismic slip distribution inversion of schemes 4–6 are shown in Table 7. In schemes 4 and 5, the sizes of regularization parameters are $\alpha_1 = 0.041$ and $\alpha_2 = 0.102$, which were determined by variance component estimation method. In scheme 2, the sizes of regularization parameters are $\alpha_1 = 0.028$ and $\alpha_2 = 0.004$, which were determined by U-curve method.

It can be seen from the data of Schemes 4 and 5 in Table 7 that the D-values between the maximum slip inversion result of WLSC and the analogue value is 0.20 m. However, the D-values between the inversion result of ASC and the analogue value is about 0.40 m, which indicates that the maximum slip inversion result of WLSC is better than the ASC. From table 8, compare with the parameters derived by the variance component estimation, the U-curve method improves the maximum slip and RMS of regularization parameter by 17.89 and 4 per cent.

4 THE INVERSION OF ACTUAL EARTHQUAKE

4.1 Slip distribution inversion of the L'Aquila earthquake

An M_w 6.3 earthquake occurred in L'Aquila, central Italy, on 2009 April 6. This earthquake caused heavy casualties and property losses (Walters *et al.* 2009; Wang *et al.* 2018a). The 1254 points of InSAR ascending data and 1282 points of InSAR descending data from Wen *et al.* (2012) are used to perform the slip distribution inversion of L'Aquila earthquake (see Fig. 9). In the L'Aquila earthquake inversion, we utilize the fault parameters (the strike angle, dip angle, the top depth etc.) from Wang *et al.* (2018b). Accordingly, the coseismic slip distribution inversion is derived from schemes 1, 2 in the simulation experiments 1. The regularization parameters were obtained by the U-curve method, and the slip distribution inversion results by schemes 1, 2 of L'Aquila earthquake are shown in Fig. 10. The slip distribution inversion results of L'Aquila earthquake by schemes 1, 2 are shown in Table 9.

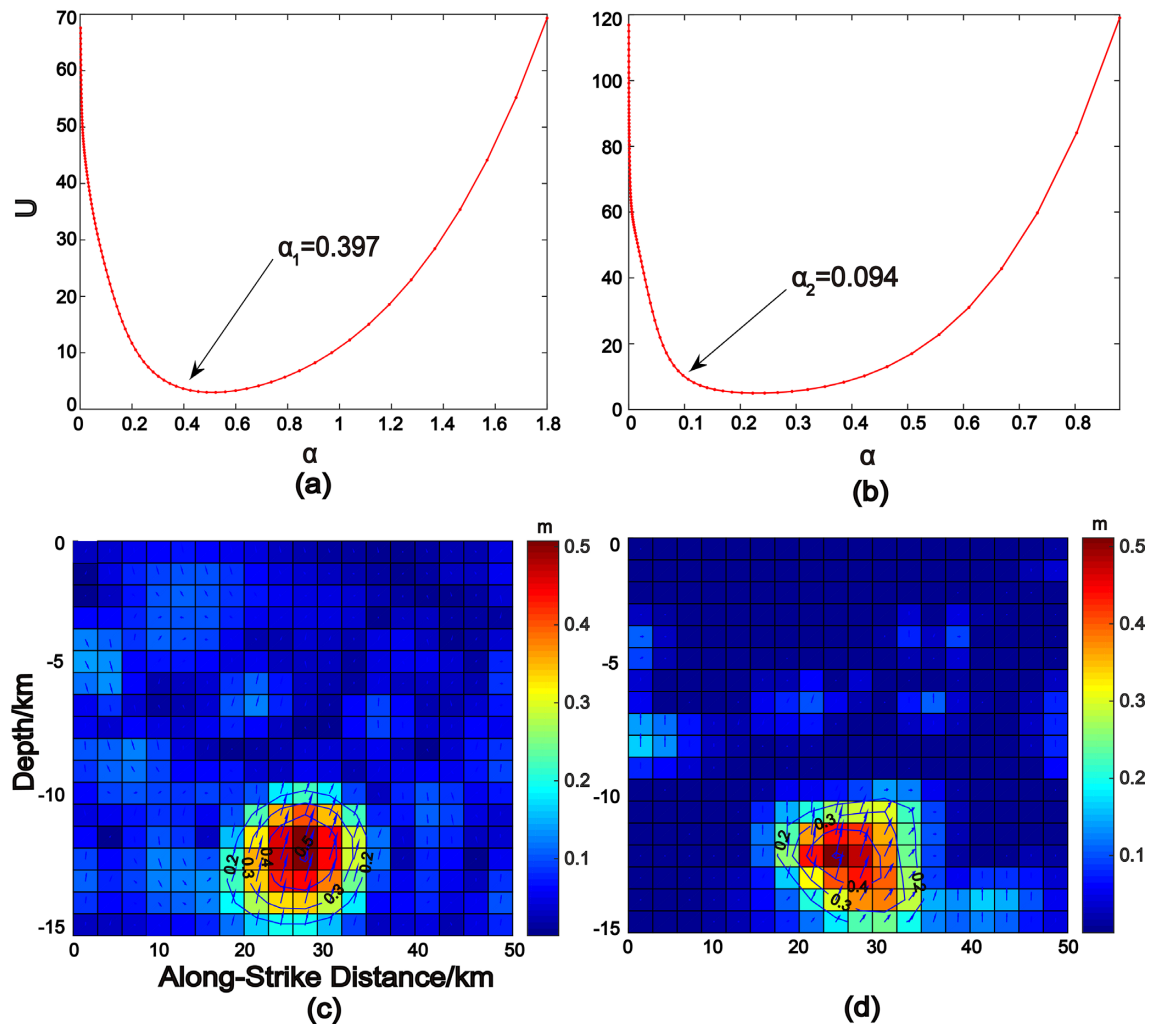


Figure 12. The slip distribution inversion results of Meinong earthquake. (a,b) The regularization parameters are determined by the U-curve method of Meinong earthquake. (c,d) The slip distribution inversion results of Meinong earthquake by schemes 1, 2.

Table 10. The various source parameters for Meinong earthquake.

Seismic parameters	Scheme 1	Scheme 2	Wang et al. (2017b)	Uniform sliding	GCMT	USGC	Huang et al. (2016)	Lee et al. (2016)
Max slip/m	0.505	0.512	0.517/0.553	//	//	//	//	//
Mean slip angle/(°)	49.5	44.7	51.5	-51.5	21	38	45	//
Moment magnitude (M_w)	6.36	6.40	6.38	6.33	6.40	6.40	6.39	6.52

Table 11. The priors information for the simulated experiment 4 by Bayesian method.

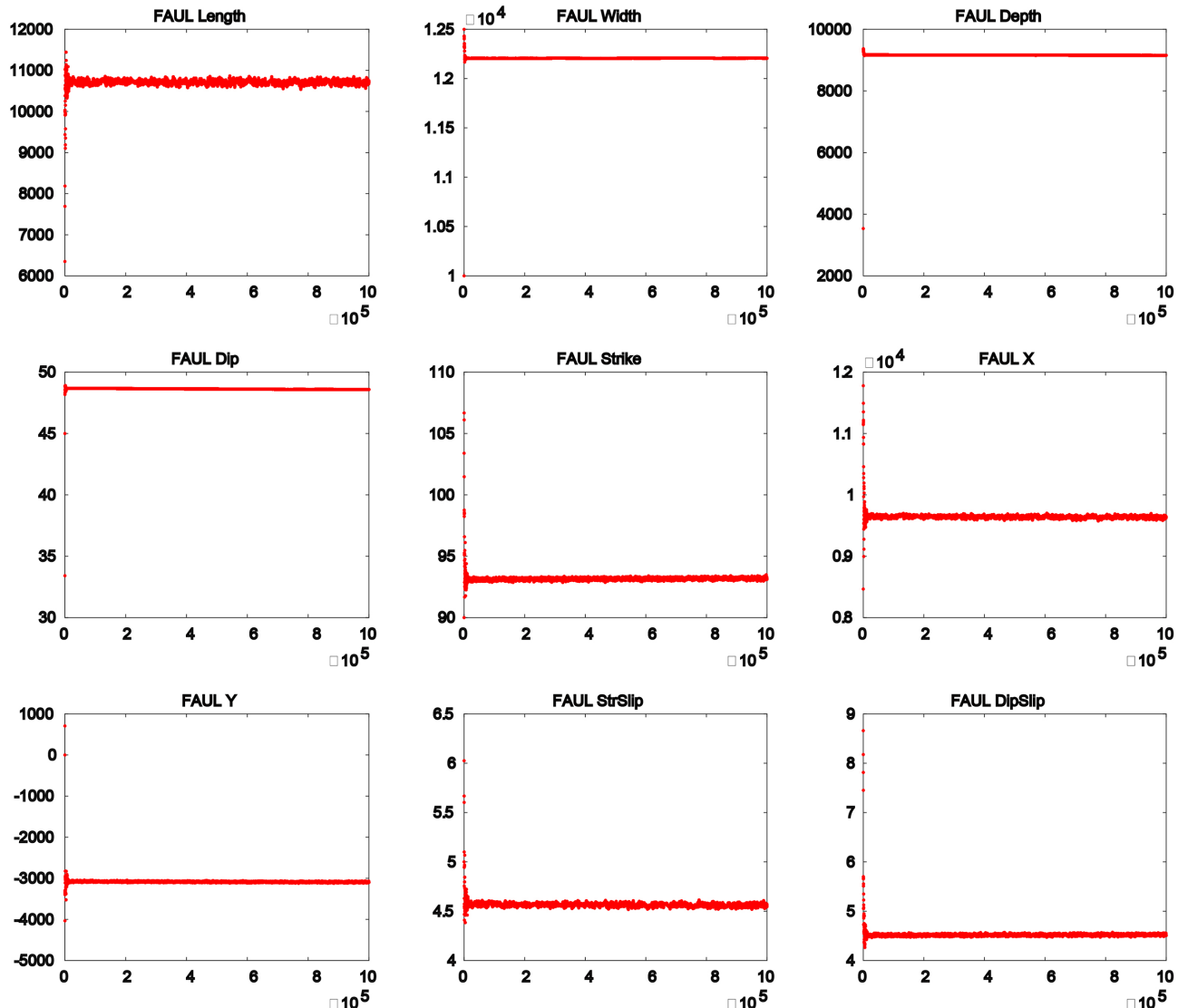
Rectangular dislocation with uniform slip (Okada, 1985)									
Fault	Length (m)	Width (m)	Z-centre (m)	Dip (°)	Strike (°)	X-centre (m)	Y-centre (m)	Strike-slip (m)	Dip-slip (m)
Start	10 000	10 000	3535	45	90	8465	0	5	8.66
Step	100	100	100	1	1	100	100	0.1	0.1
Lower bound	5000	5000	0	0	0	-20 000	-20 000	-15	-15
Upper band	20 000	20 000	20 000	90	360	20 000	20 000	15	15

Table 12. The inversion results for the simulated experiment 4 by Bayesian method.

Parameter	Analogue value	Optimal	Mean	Median	2.5 per cent	97.5 per cent
FAUL length (m)	10 000	10 710.63	10 720.91	10 712.98	10 624.60	10 798.43
FAUL width (m)	10 000	12 205.84	12 216.16	12 205.69	12 204.67	12 207.77
FAUL depth (m)	3535	9153.64	9187.05	9158.99	9153.94	9167.32
FAUL dip ($^{\circ}$)	45	48.59	48.70	48.63	48.58	48.68
FAUL strike ($^{\circ}$)	90	93.20	93.31	93.15	92.99	93.30
FAUL X (m)	8465	9636.59	9637.75	9640.60	9606.34	9674.20
FAUL Y (m)	0	-3095.50	-3082.33	-3086.08	-3107.41	-3063.78
FAUL strike-slip (m)	5	4.56	4.56	4.56	4.54	4.59
FAUL dip-slip (m)	8.66	4.52	4.51	4.52	4.49	4.55

Table 13. The coseismic slip distribution inversion results of schemes 1, 2 and Bayesian method of simulated experiment 4.

Parameters	Total slip (intermediate)	Strike-slip (intermediate)	Dip-slip (intermediate)
Analogue value	10	5	8.66
Scheme 1	9.94	4.95	8.60
Scheme 2	10.02	5.04	8.661
Bayesian method	6.42	4.56	4.52

**Figure 13.** The convergence of each parameters of Bayesian method.

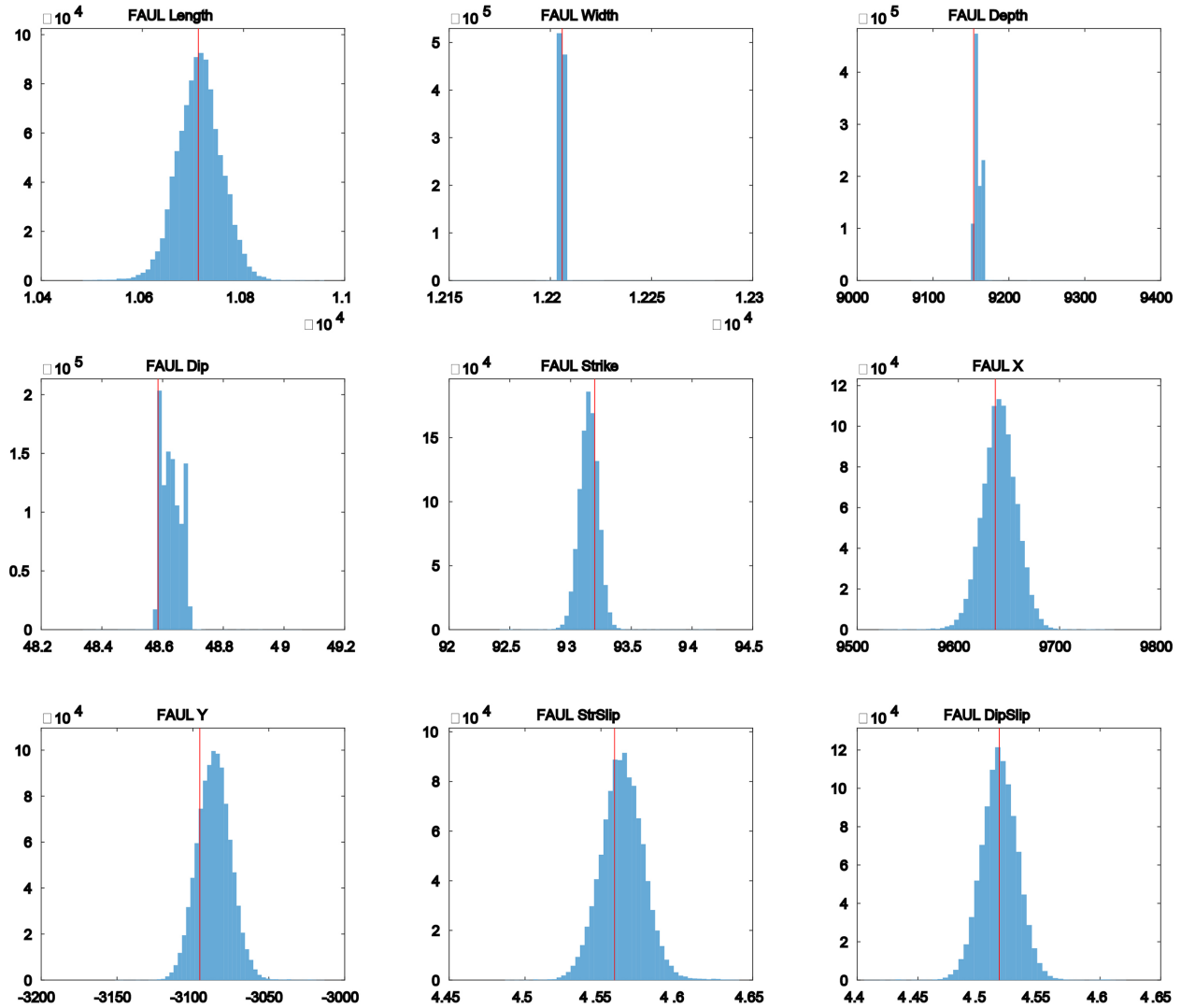


Figure 14. The probability distribution of each parameters.

In Figs 10(c),(d), the inversion results are carried out by schemes 1, 2 showing that the slip distribution area of the L'Aquila earthquake does not contain obvious slip near the surface. It is mainly distributed within 4–15 km underground. It can be seen from Table 9 that the inversion results of the L'Aquila earthquake by two schemes are within a reasonable interval of other studies (Wen *et al.* 2012; Wang *et al.* 2017a). For the maximum slip, the inversion results of schemes 1, 2 are 0.99 and 1.15 m, respectively, and the inversion result of scheme 2 is larger than that of scheme 1, which is consistent with the conclusion of the simulation experiments. Wen *et al.* (2012) combined the multiple geodetic data (the DInSAR data from Envisat and ALOS and the regional GPS data) with the elastic triangular dislocation model to invert a maximum slip at 1.07 m. The inversion results of Wen *et al.* (2012) was slightly different from this paper, which may be related to the data sources for the surface constraint. The maximum slip obtained by least-squares and total least-squares methods of Wang *et al.* (2017a) was 0.95 m, which is less than the results of this paper. The mean slip angle inversion results of schemes 1, 2 are -93.2° and -93.5° , respectively, which are slightly less than the inversion results by other studies. For the moment magnitude, the inversion results obtained by schemes 1, 2 are M_w 6.34, M_w 6.36, which are close to those reported by

other scholars. In addition, the slip inversion results of Walters *et al.* (2009) was 0.66 m, and the corresponding seismic moment was 2.80×10^{18} Nm, which were obtained by ASAR data. Cheloni *et al.* (2010) used GPS data from an observation station near the L'Aquila epicentre and studied the coseismic slip distribution of the L'Aquila earthquake and its aftershocks, the results of which revealed a maximum slip of 1.1 m and a seismic moment of 3.90×10^{18} Nm.

4.2 Slip distribution inversion of the Meinong, Taiwan earthquake

An M_w 6.4 earthquake occurred in the Meinong district of Kaohsiung City, Taiwan, China, on 2016 February 6 (Global Centroid Moment Tensor, GCMT). The Meinong earthquake caused a large number of houses to collapse and major casualties. The 225 points of GPS data from Wang *et al.* (2017b) are used to perform the Meinong earthquake slip distribution inversion in this paper (see Fig. 11). In the slip distribution inversion of Meinong earthquake, the fault parameters were obtained by Wang *et al.* (2018b) (the strike angle, dip angle, the top depth and so on). The non-negative constrained least-squares method is used to avoid contradictions

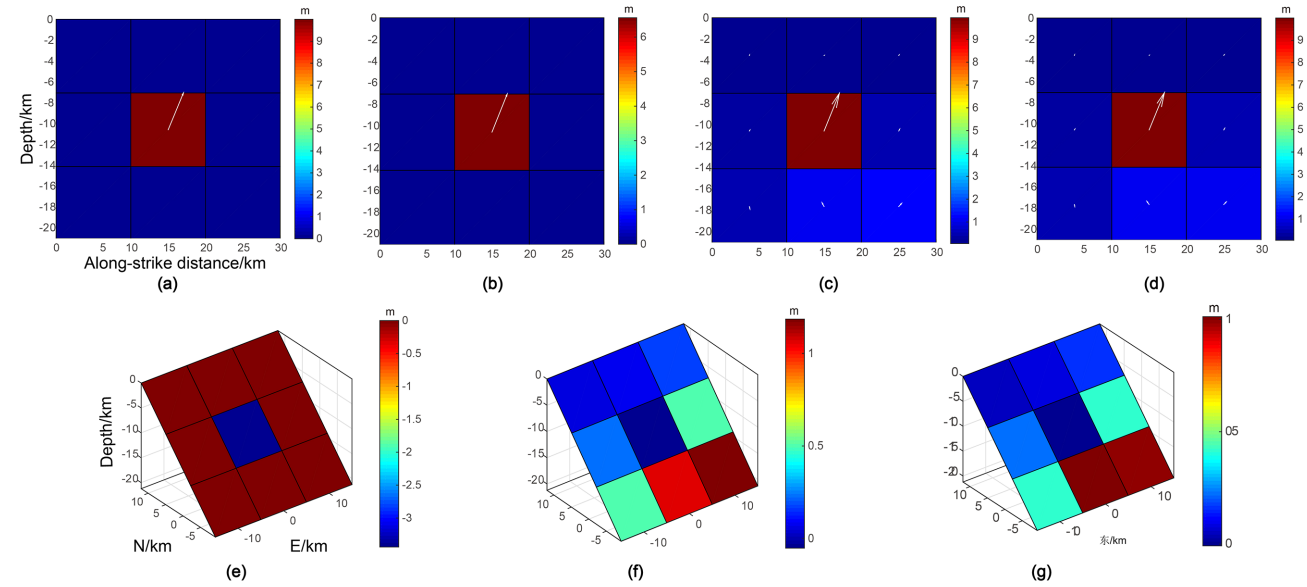


Figure 15. The slip distribution inversion results of scheme 1, scheme 2 and Bayesian method. (a) The distribution of analogue slip value. (b) The distribution of slip value of Bayesian method. (c) The distribution of slip value of scheme 1. (d) The distribution of slip value of scheme 2. (e) The residual distribution by the Bayesian method. (f) The residual distribution by the scheme 1. (g) The residual distribution by the scheme 2.

in the directions of a few sliding patches in this paper (Clerc & Kennedy 2002; Feng *et al.* 2015; Feng & Li 2010). The coseismic slip distribution inversion were carried out by using the schemes 1, 2 in the simulation experiments 1. The slip distribution inversion results by schemes 1, 2 of Meinong earthquake, and the regularization parameters determined by the U-curve method are shown in Fig. 12. The Meinong earthquake slip distribution inversion results of the schemes 1, 2 are shown in Table 10.

In Figs 12(c),(d), the inversion results are carried out by schemes 1, 2 showing that the slip distribution area of the Meinong earthquake is distributed within the range of 9–14 km underground and does not extend to the surface, which are consistent with the no obvious surface rupture found in ground. In Table 10, for the maximum slip, the inversion results of schemes 1, 2 are 0.505 and 0.512 m, respectively, and the inversion result of scheme 2 is larger than that of scheme 1, which is consistent with the conclusion of the simulation experiments. Wang *et al.* (2017b) combined with InSAR and GPS data to invert the Meinong earthquake, and the inversion results show that the maximum dip-slip and maximum strike-slip are 0.517 and 0.553 m, respectively, which are slightly larger than the inversion results of the schemes 1, 2. The inversion results of mean slip angle of the two schemes are 49.5° and 44.7°, respectively. The multifault models which were constructed in Huang *et al.* (2016) are a good way to restore seismic wave and GPS data, but the InSAR data does not fit well. Huang *et al.* (2016) determined the geometric parameters of large faults by using GPS and seismic data firstly, and used InSAR data residuals to fit the shallow small faults for inversion. The mean slip angle of the inversion is 45°, which is similar to the inversion result by scheme 2 in this paper. The inversion result of scheme 1 is between the results of Wang *et al.* (2017b) and Huang *et al.* (2016). The inversion results of the moment magnitude by two schemes are within the scope of other scholars. The moment magnitude result of the inversion of Lee *et al.* (2016) was M_w 6.52. The reason that the inversion result is larger than those of other scholars may be related to the lack of fitting GPS data well (Wang *et al.* 2017b).

5 DISCUSSION AND CONCLUSIONS

We present a new method, namely weighing to Laplace second-order smoothness matrix by slip (WLSC), for the inversion of coseismic slip distribution. We test our method on both system simulation experiments and realistic earthquakes. The inversion results of the simulation experiment 1 indicate that the fault depth will affect the inversion accuracy significantly. Accordingly, with the fault depth going deeper, the inversion accuracy is degraded. Simulation experiment 1 also verifies that the inversion accuracy of the coseismic slip distribution inversion via WLSC can improve the inversion accuracy of the maximum slip which is not related to the redetermination of the regularization parameter as well. In order to make the simulation experiment more realistic, the simulation experiment 2 designed a coseismic slip distribution inversion experiment with double main sliding areas. The inversion results show that the more complex the fault sliding area, the lower the accuracy of parameters of coseismic slip distribution inversion. It can be concluded from the inversion results of simulation experiments 1, 2 that the proposed WLSC method is better than the classic LSC in all cases (e.g. different fault sliding areas and fault depths). The inversion results of simulation experiment 3 also show that the inversion accuracy of the WLSC is better than ASC (Fan *et al.* 2017). In general, the WLSC can improve the overall accuracy by 12–19 per cent comparing with the LSC method.

The inversion results of simulation experiments 1, 2 and 3 show that the inversion results of slip distribution with WLSC are higher than the inversion of LSC in the maximum slip, average slip and moment magnitude parameters, especially for the maximum slip inversion accuracy. The simulation experiments inversion results show that the inversion results of WLSC are improved by 12–19 per cent compared with LSC. The reason is that using the method of this paper to weigh the Laplacian second-order smoothness matrix can ensure that the larger the slip of the fault patch is, the smaller the corresponding weight is. For the maximum slip, the weight of the surrounding sliding patches is larger than it. From formula (6), it can be seen that the maximum slip inversion value can be theoretically improved and can solve the problem of underestimating the

maximum slip of LSC. For the mean slip and moment magnitude parameters, the inversion results of WLSC are improved by 4–12.5 and 0.4–9 per cent compared with the LSC, respectively.

In addition, this paper performed the slip distribution inversion for 2009 L'Aquila actual earthquake and 2016 Meinong earthquake using WLSC and LSC methods. The inversion results show that the maximum slip inversion results WLSC is larger than the inversion result of LSC, which is consistent with the simulation experiments. Besides, the parameters of inversion results such as mean slip and moment magnitude are similar to other studies. Therefore, the inversion results of L'Aquila and Taiwan's Meinong earthquakes show that it is feasible and effective to use the WLSC for coseismic slip distribution inversion.

The inversion results of simulation experiments and the actual earthquake show that the slip distribution inversion of WLSC can improve the parameters accuracy of coseismic slip distribution inversion, which provides a better understanding of the rupture process of earthquake source. Since the slip distribution model is the basis of coseismic Coulomb stress change calculation and fault stress interaction analysis, the higher accuracy of parameters inversion also facilitate the study of seismic strain accumulation, post-earthquake sliding mode and earthquake disaster prediction and rescue.

Moreover, the ill-posed problem in coseismic slip distribution inversion can be solved by the Markov chain Monte Carlo method (Simons *et al.* 2011). In experiment 4, we compared our method with Monte Carlo method implementing in Geodetic Bayesian Inversion Software (GBIS – Version 1.1) from Bagnardi & Hooper (2018). The GBIS integrates Markov-chain Monte Carlo algorithm and the Metropolis–Hastings algorithm (e.g. Hastings 1970; Mosegaard & Tarantola 1995) to find out the posterior probability distribution of the different source parameters. A detailed explanation of the inversion approach is provided in Bagnardi & Hooper (2018). In brief, the Bayesian method is a method of treating the fault plane as a uniform surface, then the probability distribution of the fault plane parameters (fault length, width, dip angle, strike angle) will be obtained (Bagnardi & Hooper 2018). Since the method considers the fault plane as a uniform plane, it has the advantage of not requiring the additional Laplacian smoothing constraints as well as the regularization parameters determination. The specific fault parameters in experiment 4 are set as follows: The length and width of fault are 30 km, the dip angle is 45°, the strike angle is 90°. The fault plane is divided into 3*3 patches, and the most intermediate sliding patch was given a sliding amount of 10 m, the sliding angle is 60°. The 400 surface observation points were simulated in the range of X (−10–10 km) and Y (−10–10 km). Since the sliding value only assigned to the intermediate sliding patch on the fault plane, the length and width of the most intermediate sliding patch are 10 km. The schemes1, schemes 2 and Bayesian method are used to invert slip distribution. The prior information of parameters by Bayesian method are set in Table 11, and the probability distribution results of each parameters are shown in Table 12. The convergence of each parameters of Bayesian method are shown in Fig. 13. The probability distributions of each parameter are shown in Fig. 14.

It can be seen from Figs 13, 14 that each parameter reaches convergences, and most of the parameters are subject to the normal distribution. Thus, the calculation result is considered to be credible. From Table 12, the optimal value of strike-slip of intermediate patch calculated by Bayesian method is 4.56 m, and the optimum value of dip-slip of intermediate patch calculated by Bayesian method is 4.52 m.

In addition, the coseismic slip distribution inversion results of schemes 1, 2 and Bayesian method are shown in Fig. 15, and slip parameters inversion results of above methods are shown in Table 13.

According to the result of experiment 4 (see Table 13 and Fig. 15), the WLSC method achieves highest accuracy in most sliding patches. The slip value obtained by schemes1 and 2 are superior to the Bayesian method.

This paper proposes a method for coseismic slip distribution inversion, namely WLSC, to improve the classic LSC method through a novel weighing strategy according to the slip. The experiments from both simulating and actual earthquake data demonstrate the effectiveness and performance of the proposed method comparing with other methods. In future work, we intend to consider different weighing methods of WLSC for various applications. In addition, a combination of Bayesian method and WLSC is worthy to be investigated to obtain a more comprehensive parameter inversion results.

ACKNOWLEDGEMENTS

We thank the anonymous reviewers for their careful reading and precious suggestions. This research is supported by the National Natural Science Foundation of China (Nos. 41874001, 41664001 and 41204003), the Support Program for Outstanding Youth Talents in Jiangxi Province (No. 2016BCB23050), the National Key Research and Development Program (No. 2016YFB0501405).

REFERENCES

- Allen, D.M., 1974. The relationship between variable selection and data agumentation and a method for prediction, *Technometrics*, **16**(1), 25–127.
- Amey, R.M.J., Hooper, A. & Walters, R.J., 2018. A Bayesian method for incorporating self-similarity into earthquake slip inversions, *J. geophys. Res.*, **123**, 6052–6071.
- Amiri-Simkooei, A.R., 2016. Non-negative least-squares variance component estimation with application to GPS time series, *J. Geod.*, **90**(5), 451–466.
- Ammon, C.J. *et al.* 2005. Rupture process of the 2004 Sumatra-Andaman earthquake, *Science*, **308**(5725), 1133–1139.
- Anzidei, M. *et al.* 2009. Coseismic deformation of the destructive April 6, 2009 L'Aquila earthquake (Central Italy) from GPS data, *Geophys. Res. Lett.*, **36**(17): L17307, doi:10.1029/2009GL039145.
- Arnrich, S., Brüer, P., Klauck, M. & Kalies, G., 2014. Suitability of L- and U-curve methods for calculating reasonable adsorption energy distributions from Nitrogen Adsorption Isotherms, *Adsorption Sci. Technol.*, **32**(7), 521–534.
- Arthur, E.H. & Robert, W.K., 1970. Ridge regression: biased estimation for nonorthogonal problems, *Technometrics*, **8**(1), 27–51.
- Bagnardi, M. & Hooper, A., 2018. Inversion of surface deformation data for rapid estimates of source parameters and uncertainties: a Bayesian approach, *Geochem. Geophys. Geosyst.*, **19**, 2194–2211.
- Chamorroservent, J., Aguirre, J. & Ripoll, J., 2011. Feasibility of U-curve method to select the regularization parameter for fluorescence diffuse optical tomography in phantom and small animal studies, *Opt. Express*, **19**(12), 11490–506.
- Cheloni, D. *et al.* 2010. Coseismic and initial post-seismic slip of the 2009 Mw6.3 L'Aquila earthquake, Italy, from GPS measurements, *Geophys. J. Int.*, **181**(3), 1539–1546.
- Chen, Q., Cheng, H., Yang, Y., Liu, G. & Liu, L., 2014. Quantification of mass wasting volume associated with the giant landslide Daguangbao induced by the 2008 Wenchuan earthquake from persistent scatterer InSAR, *Remote Sens. Environ.*, **152**, 125–135.
- Clerc, M. & Kennedy, J., 2002. *The Particle Swarm-Explosion, Stability, and Convergence in a Multidimensional Complex Space*. IEEE Press.

- Delouis, B., Nocquet, J.M. & Vallée, M., 2010. Slip distribution of the February 27, 2010 Mw = 8.8 Maule Earthquake, central Chile, from static and high-rate GPS, InSAR, and broadband teleseismic data, *Geophys. Res. Lett.*, **37**, L17305, doi:10.1029/2010GL043899.
- Desbrun, M., Meyer, M., Schröder, P. & Barr, A.H., 1999. Implicit fairing of irregular meshes using diffusion and curvature flow, in *Proc. SIGGRAPH '99 Proceedings of the 26th Annual Conference on Computer Graphics and Interactive Techniques*, Vol. **99**, ACM Press/Addison-Wesley Publishing Co., New York, pp. 317–324.
- Diao, F., Walter, T.R., Solaro, G. et al. 2016. Fault locking near Istanbul: indication of earthquake potential from InSAR and GPS observations, *Geophys. J. Int.*, **205**(1), 490–498.
- Fan, Q., Xu, C., Yi, L., Liu, Y., Wen, Y. & Yin, Z., 2017. Implication of adaptive smoothness constraint and Helmert variance component estimation in seismic slip inversion, *J. Geod.*, **91**, 1163–1177.
- Feng, G., Li, Z., Shan, X., Zhang, L., Zhang, G. & Zhu, J., 2015. Geodetic model of the 2015 April 25 M_w 7.8 Gorkha Nepal earthquake and M_w 7.3 aftershock estimated from InSAR and GPS data, *Geophys. J. Int.*, **203**(2), 896–900.
- Feng, W.P. & Li, Z.H., 2010. A novel hybrid PSO /simplex algorithm for determining earthquake source parameters using InSAR data, *Process Geophys.*, **25**(4), 1189–1196.
- Funning, G.J., Parsons, B., Wright, T.J., Jackson, J.A. & Fieldin, E.J., 2005. Surface displacements and source parameters of the 2003 Bam (Iran) earthquake from Envisat advanced synthetic aperture radar imagery, *J. geophys. Res.*, **110**(B9), 259–259.
- Golub, G.H., Heath, M. & Wahba, G., 1979. Generalized cross-validation as a method for choosing a good ridge parameter, *Technometrics*, **21**(2), 215–223.
- Grafarend, E.W., 1985. Variance-covariance component estimation, *Theoret. Results Geod. Appl. Statist Decisions*, (Suppl 2), 407–441.
- Hansen, P.C., 1992. Analysis of discrete III-posed problems by means of the l-curve, *SIAM Rev.*, **34**(4), 561–580.
- Hansen, P.C. & O'Leary, D.P., 1993. The use of the L-curve in the regularization of discrete ill-posed problems, *SIAM J. Sci. Comput.*, **14**(6), 1487–1503.
- Hastings, W.K., 1970. Monte Carlo sampling methods using Markov chains and their applications, *Biometrika*, **57**(1), 97–109.
- Helmut, F.R., 1872. Die Ausgleichungsrechnung nach der Methode der Kleinsten Quadrate, mitanwendungen auf die geodasie und die theorie der messinstrumente. Teubner.
- Huang, M.H., Tung, H., Fielding, E.J., Huang, H.-H., Liang, C., Huang, C. & Hu, J.-C., 2016. Multiple fault slip triggered above the 2016 M_w 6.4 Meinong earthquake in Taiwan, *Geophys. Res. Lett.*, **43**, 7459–7467.
- Jiang, G., Xu, C., Wen, Y., Liu, Y., Yin, Z. & Wang, J., 2013. Inversion for coseismic slip distribution of the 2010 Mw 6.9 Yushu earthquake from InSAR data using angular dislocations, *Geophys. J. Int.*, **194**(2), 1011–1022.
- Jiang, Z.S. et al. 2014. GPS Constrained coseismic source and slip distribution of the 2013 Mw6.6 Lushan, China, earthquake and its tectonic implications, *Geophys. Res. Lett.*, **41**(2), 407–413.
- Ji, C., Helmberger, D.V., Wald, D.J. & Ma, K., 2003. Slip history and dynamic implications of the 1999 Chi-Chi, Taiwan, earthquake, *J. geophys. Res.*, (1978–2012): 369–378.
- Ji, C., Wald, D.J. & Helmberger, D.V., 2002. Source description of the 1999 hector mine, California, earthquake, Part I: wavelet domain inversion theory and resolution analysis, *Bull. seism. Soc. Am.*, **92**(4), 1192–1207.
- Jónsson, S., Zebker, H., Segall, P. & Amelung, F., 2002. Fault slip distribution of the 1999 M_w 7.1 hector mine, California, earthquake, estimated from satellite radar and GPS measurements, *Bull. seism. Soc. Am.*, **92**, 1377–1389.
- Kasahara, K., 1957. The nature of seismic origins as inferred from seismological and geodetic observations, *Bull. Earthq. Res. Inst.*, **35**, 473–532.
- Kobayashi, T., Tobita, M., Nishimura, T., Suzuki, A., Noguchi, Y. & Yamamoto, M., 2011. Crustal deformation map for the 2011 off the Pacific coast of Tohoku Earthquake, detected by InSAR analysis combined with GEONET data, *Earth Planets Space*, **63**(7), 621–625.
- Krawczyk-Stando, D. & Rudnicki, M., 2007. Regularization parameter selection in discrete ill-posed problems—the use of the U-curve, *Int. J. Appl. Math. Comput. Sci.*, **17**(2), 157–164.
- Lee, S.J., Yeh, T.Y. & Lin, Y.Y., 2016. Anomalously large ground motion in the 2016 ML 6.6 Meinong, Taiwan, earthquake: a synergy effect of source rupture and site amplification, *Seismol. Res. Lett.*, **87**(6), 1–8.
- Liu, J., Ding, L., Ji, C. et al. 2009. Coseismic ruptures of the 12 May, 2008, Ms 8.0 Wenchuan earthquake, Sichuan: East-west crustal shortening on oblique, parallel thrusts along the eastern edge of Tibet, *Earth planet. Sci. Lett.*, **286**, 355–370.
- Maerten, F., Resor, P., Pollard, D. & Maerten, L., 2005. Inverting for slip on three-dimensional fault surfaces using angular dislocations, *Bull. seism. Soc. Am.*, **95**(5), 1654–1665.
- Mosegaard, K. & Tarantola, A., 1995. Monte Carlo sampling of solutions to inverse problems, *J. geophys. Res.*, **100**, 12 431–12 447.
- Okada, Y., 1985. Surface deformation to shear and tensile faults in a half-space, *Bull. seism. Soc. Am.*, **75**(4), 1135–1154.
- Okada, Y., 1992. Internal deformation due to shear and tensile fault in a half space, *Bull. seism. Soc. Am.*, **92**(2), 1018–1040.
- Pollitz, F.F. et al. 2011. Coseismic slip distribution of the February 27, 2010 M_w 8.8 Maule, Chile earthquake, *Geophys. Res. Lett.*, **38**(9), L09309, doi:10.1029/2011GL047065.
- Savage, J. & Hastie, L., 1969. A dislocation model for the Fairview peak, Nevada, earthquake, *Bull. seism. Soc. Am.*, **5**, 1937–1948.
- Simons, M. et al. 2011. The 2011 magnitude 9.0 Tohoku-Oki earthquake: mosaicking the megathrust from seconds to centuries, *Science*, **332**, 1421–1425.
- Stone, M., 1974. Cross-validatory choice and assessment of statistical predictions, *J. R. Stat. Soc. B*, **36**(2), 111–147.
- Sun, W., Okubo, S. & Vaníček, P., 1996. Global displacements caused by point dislocations in a realistic Earth model, *J. geophys. Res.*, **101**(4), 8561–8578.
- Tajima, F., Mori, J. & Kennett, B.L.N., 2013. A review of the 2011 Tohoku-Oki earthquake (Mw 9.0): large-scale rupture across heterogeneous plate coupling, *Tectonophysics*, **586**(586), 15–34.
- Tikhonov, A.N., 1963. Regularization of incorrectly posed problems, *Sov. Math.*, **4**(1), 1624–1627.
- Tikhonov, A.N. & Arsenin, V.Y., 1977. Solutions of ill-posed problems, *Math. Comput.*, **32**(144), 491–491.
- Walters, R.J. et al. 2009. The 2009 L'Aquila Earthquake (Central Italy): a source mechanism and implications for seismic hazard, *Geophys. Res. Lett.*, **36**, 17, doi:10.1029/2009GL039337.
- Wang, C., Ding, X., Li, Q. & Shan, X., 2016. Adaptive regularization of earthquake slip distribution inversion, *Tectonophysics*, **675**, 181–195.
- Wang, L.Y., Gao, H. & Feng, G.C., 2017b. InSAR and GPS inversion for source parameters of the 2016 Mw6.4 Meinong, Taiwan earthquake, *Chin. J. Geophys.*, **60**(7), 2578–2588.
- Wang, L.Y., Gao, H., Feng, G.C. & Xu, W.B., 2018a. Source parameters and triggering links of the earthquake sequence in central Italy from 2009 to 2016 analyzed with GPS and InSAR data, *Tectonophysics*, **744**, 285–295.
- Wang, L.Y., Li, H.Y., Wen, Y.M. & Xu, C.J., 2017a. Total least squares method inversion for coseismic slip distribution, *Acta Geod. Cartograph. Sin.*, **46**(3), 307–315.
- Wang, L.Y., Zhao, X. & Gao, H., 2018b. A method for determining the regularization parameter and the relative weight ratio of the seismic slip distribution with multi-source data, *J. Geodyn.*, **118**(7), 1–10.
- Wang, Z.J., 2003. The research on the regularization method of discomfort in geodetic measurement, *Institute of Measurement and Geophysics of the Chinese Academy of Sciences*.
- Wan, Y., Shen, Z.K., Bürgmann, R., Sun, J. & Wang, M., 2017. Fault geometry and slip distribution of the 2008 Mw 7.9 Wenchuan, China earthquake, inferred from GPS and InSAR measurements, *Geophys. J. Int.*, **208**(2), 748–766.
- Wen, Y.M., He, P., Xu, C.J. & Yang, L., 2012. Source parameters of the 2009 L'Aquila earthquake, Italy from Envisat and ALOS Satellite SAR Images, *Chin. J. Geophys.*, **55**(1), 53–65.
- Xu, C., Ding, K. & Cai, J., 2009. Methods of determining weight scaling factors for geodetic–geophysical joint inversion, *J. Geodyn.*, **47**(1), 39–46.

- Xu, C., Liu, Y., Wen, Y. & Wang, R., 2010. Coseismic slip distribution of the 2008 Mw 7.9 Wenchuan earthquake from joint inversion of GPS and InSAR data, *Bull. seism. Soc. Am.*, **100**(5B), 2736–2749.
- Xu, P.L., 1998. Truncated SVD methods for discrete linear ill-posed problems, *Geophys. J. Int.*, **135**(2), 505–514.
- Xu, W., Feng, G., Meng, L., Zhang, A., Ampuero, J.P., Bürgmann, R. & Fang, L., 2018. Transpressional rupture cascade of the 2016 M_w 7.8 Kaikoura Earthquake, New Zealand, *J. geophys. Res.*, **123**, 2396–2409.
- Yagi, Y. & Fukahata, Y., 2008. Importance of covariance components in inversion analyses of densely sampled observed data: an application to waveform data inversion for seismic source processes, *Geophys. J. Int.*, **175**(1), 215–221.
- Yagi, Y. & Fukahata, Y., 2011. Introduction of uncertainty of Green's function into waveform inversion for seismic source processes, *Geophys. J. Int.*, **186**, 711–720.
- Zhao, D., Qu, C., Shan, X., Gong, W., Zhang, Y. & Zhang, G., 2018. InSAR and GPS derived coseismic deformation and fault model of the 2017 Ms7.0 Jiuzhaigou earthquake in the Northeast Bayanhar block, *Tectonophysics*, **726**, 86–99.
- Zhong, Y., Wu, Y., Zhang, L. & Xu, X., 2014. Adaptive map sub-pixel mapping model based on regularization curve for multiple shifted hyperspectral imagery, *ISPRS J. Photogramm. Remote Sens.*, **96**(4), 134–148.